Colloids and Surfaces B: Biointerfaces 77 (2010) 181–190

Contents lists available at ScienceDirect

Colloids and Surfaces B: Biointerfaces

journal homepage: www.elsevier.com/locate/colsurfb

Effect of nanoscale topography on fibronectin adsorption, focal adhesion size and matrix organisation

Cristina González-García[a], Susana R. Sousa[b,c], David Moratal[a], Patricia Rico[a,d,*], Manuel Salmerón-Sánchez[a,d,e,*]

[a] Center for Biomaterials and Tissue Engineering, Universidad Politécnica de Valencia, 46022 Valencia, Spain
[b] INEB – Instituto de Engenharia Biomédica, Div. Biomateriais, Porto, Portugal
[c] ISEP – Instituto Superior de Engenharia do Porto, Dep. Engenharia Química, Porto, Portugal
[d] Networking Research Center on Bioengineering, Biomaterials and Nanomedicine (CIBER-BBN), Valencia, Spain
[e] Regenerative Medicine Unit, Centro de Investigación Príncipe Felipe, Autopista del Saler 16, 46013 Valencia, Spain

ARTICLE INFO

Article history:
Received 30 September 2009
Received in revised form
21 December 2009
Accepted 28 January 2010
Available online 4 February 2010

Keywords:
Nanotopography
Protein adsorption
Cell adhesion
Fibronectin

ABSTRACT

Phase separation of PLLA/PS (50/50, w/w) solutions during a spin-casting process gives rise to well-defined nanotopographies of 14, 29 and 45 nm deep pits depending on the concentration of the solution. Their influence on the biological activity of fibronectin (FN) was investigated. FN adsorption was quantified by radiolabelling the protein. The amount of adsorbed FN was higher on the 14 nm deep pit nanotopography than on the other two surfaces. FN distribution between valleys and peaks was investigated by AFM combined with image analysis. FN tends to adsorb preferentially on the valleys of the nanotopography only for the 14 nm system and when adsorbed from solutions of concentration lower than 10 μg/ml. Higher concentration of the FN solution leads to evenly distribution of the protein throughout the surface; moreover, there is no difference in the distribution of the protein between valleys and peaks for the other two systems (29 and 45 nm) irrespective of the concentration of the FN solution. The biological activity of the adsorbed protein layer was assessed by investigating MC3T3 osteoblast-like cells adhesion, FN reorganisation and late matrix formation on the different substrates. Even if initial cell adhesion is excellent for every substrate, the size of the focal adhesion plaques increases as the size of the pits in the nanotopography does. This is correlated to FN reorganisation, which only takes places on the 29 and 45 nm deep pits surfaces, where enhanced late matrix production was also found.

1. Introduction

The initial cellular events that take place at the biomaterials interface mimic to a certain extent the natural adhesive interaction of cells with the extracellular matrix (ECM) [1–3]. In fact, the living cells cannot interact directly with foreign materials, but they readily attach to the adsorbed protein layer of proteins such as fibronectin (FN), vitronectin (VN), fibrinogen (FNG), representing the so-called soluble matrix proteins in the biological fluids [3]. Upon longer contact with tissues many other ECM proteins, such as collagens and laminins, will also associate with the surfaces, affecting the cellular interaction. Cells recognize these matrix proteins via integrins – a family of cell surface receptors – that provide trans-membrane links between the ECM and the actin cytoskeleton [4]. When integrins are occupied they cluster and develop focal adhesion complexes that actually anchorage the cells to the surface and trigger the subsequent cellular response [4]. Thus, the initial cell–material interaction is a complex multi-step process consisting of early events, such as adsorption of proteins, followed by cell adhesion and spreading, and late events, related to cell growth, differentiation, matrix deposition and cell functioning.

Even if the cell–material interaction is not a direct one, but it is mediated by ECM proteins previously adsorbed on the substrate's surface, it is said that cells response to three different kind of surface parameters: chemical, topographical and mechanical [5,6]. Surface topography is a key parameter that is able to modify cell response independently of the chemical composition of the substrate. Even though sometimes topography is only a manifestation of material chemistry, many times it can be modulated in an independent way. The effect of topography on cell adhesion has been widely studied. Micro and nanopatterned surfaces have been prepared for a better understanding of the cell response to topographic features, mainly in what cell adhesion is concerned. Anisotropic surfaces prepared by lithographic and microfabrication techniques can induce cell reorientation follow-

* Corresponding authors: Center for Biomaterials and Tissue Engineering, Universidad Politécnica de Valencia, 46022 Valencia, Spain. Tel.: +34 963877275; fax: +34 963877276.
E-mail addresses: parico@upvnet.upv.es (P. Rico), masalsan@fis.upv.es (M. Salmerón-Sánchez).

0927-7765/$ – see front matter © 2010 Elsevier B.V. All rights reserved.
doi:10.1016/j.colsurfb.2010.01.021

ing microgrooves, the so-called contact guidance phenomenon [7,8]; and the scale of anisotropic topography plays an important role in deciding cell alignment [9]. Different techniques have been used to produce controlled isotropic topographies at different scales which include photolithography, electron beam lithography, colloidal lithography, and polymer demixing techniques during a high-speed spin-casting process [10–13] which allows obtaining nanotopographic motifs in a broad range (from 9 to 100 nm). However, the effect of nanotopography on cell response remains an open question. It seems that the interval 10–30 nm gives rise to better adhesion and higher stimulation of intracellular signalling than going up to 100 nm [14–16]. Cell differentiation and gene expression are also influenced by surface topography [17–19]. Though the effect of surface nanotopography on cell behavior should be a consequence of different protein adsorption patterns, scarce experimental data exist on the effect of surface nanotopography on protein adsorption. It has been suggested that nanotopography is able to enhance protein adsorption as compared to the same plane chemistry [20], although other claim little effect of surface nanoroughness on protein adsorption [21]. Different substrates have been prepared in the recent years aiming at investigating the role of surface nanotopography in the cell–material interaction, especially in what cell adhesion is concerned. These works are mainly focused on investigating the effect of material properties on the biological performance of the substrate and, only a few of them, investigate this effect by addressing first protein adsorption and conformation on the material surface and then by correlating this phenomenon with cell behavior.

Recently, nanoscale topographies have been prepared by using PLLA and PS demixing techniques [14]. Randomly distributed nanoscale pits (14, 29 and 45 nm deep pits) were produced by adjusting PLLA/PS at 50/50 (w/w) but varying the concentration of the spin-casting solution. It was suggested that cell attachment, cell spreading, integrin subunit expression, paxillin synthesis and FAK expression (and its phosphorylation) were enhanced on 14 and 29 nm deep pits compared to 45 nm deep pits or flat PLLA surfaces, which suggested that nanostructures provide physical signals that regulate cell function. In this work we have further investigated the role of these nanostructured PLLA/PS nanotopographies on initial cell adhesion by paying special attention to the adsorbed protein layer as the biological interface between the synthetic substrate and the cell population. We have quantified the amount of FN adsorbed on the different nanotopographies from solutions of different concentrations by radiolabelling the protein; the conformation and distribution of FN on the synthetic surfaces was directly observed by atomic force microscopy (AFM). Further, initial cell adhesion on the different FN-coated nanostructured surfaces was investigated, as well as the reorganisation of the adsorbed FN layer (after 3 h) and late matrix production as a function of time (after 1, 3 and 6 days).

2. Materials and methods

2.1. Preparation of nanotopographies

Nanoscale topographies were prepared by polymer demixing techniques as described elsewhere [14]. Briefly, PLLA (Cargill Dow) and PS (Sigma–Aldrich) were dissolved in chloroform at fixed polymer composition 50/50 (w/w) and different total polymer concentration (0.5, 1, and 1.5%). Spin casting was performed on 12 mm glass coverslips at 4000 rpm for 30 s. Pure PLLA was also spin-casted from a 2% solution with similar conditions (2000 rpm for 30 s). Samples were dried in vacuo at room temperature before further characterisation.

2.2. Atomic force microscopy (AFM)

AFM experiments were performed using a Multimode AFM equipped with NanoScope IIIa controller from Veeco (Manchester, UK) operating in tapping mode in air; the Nanoscope 5.30r2 software version was used. Si-cantilevers from Veeco (Manchester, UK) were used with force constant of 2.8 N/m and resonance frequency of 75 kHz. The phase signal was set to zero at a frequency of 5–10% lower than the resonance one. Drive amplitude was 600 mV and the amplitude setpoint A_{sp} was 1.8 V. The ratio between the amplitude setpoint and the free amplitude A_{sp}/A_0 was kept equal to 0.8.

Fibronectin from human plasma (Sigma, Barcelona, Spain) was adsorbed on the different substrates by immersing the material sheets in several FN solutions at concentrations of 2, 5, 10 and 20 μg/ml in physiological solution (NaCl 0.9%) for 10 min. After protein adsorption, samples were rinsed in the physiological solution to eliminate the non-adsorbed protein. Remaining drops on the surface were dried by exposing the sample to a nitrogen flow for 2–3 min. AFM was performed in the tapping mode in air immediately after sample preparation. Height, phase and amplitude magnitudes were recorded simultaneously for each image.

2.3. Protein quantification by radioactivity

The amount of adsorbed FN in equilibrium was quantified by radiolabelling the protein with ^{125}I using the Iodogen Method [22,23]. Thereafter ^{125}I-FN was passed through Sephadex column G-25 M (PD-10 desalting column, Amersham Pharmacia Biotech) to remove unbound ^{125}I. The yield of iodination in different fractions was determined by precipitating the ^{125}I-labelled FN with 20% trichloroacetic acid (TCA method). Only fractions with yield of iodination higher than 98% were used.

The contribution of free ^{125}I to the total radioactivity found on the surfaces was estimated using unlabelled FN solutions at a concentration of 1.0 mg/ml and an amount of free ^{125}I ion equivalent to that present as ^{125}I ion in the labelled protein solutions.

In all studies in which radiolabelling methods are used it must be kept in mind that the behavior of the labelled protein may or may not reflect the behavior of unlabelled protein. To assess whether preferential adsorption of ^{125}I-labelled FN occurred on surfaces, a series of control experiments were performed in previous studies by varying the ratio of labelled to unlabelled FN (10–50%). The final concentration of the FN solutions (1.0 mg/ml) was confirmed by the bicinchoninic acid (BCA) assay using a BCA assay kit from Pierce and bovine serum albumin (BSA) as the standard [23]. Protein solutions for adsorption experiments were prepared by adding (^{125}I-FN) to unlabelled FN solution to obtain a final activity of 10^7 cpm/mg.

FN adsorption tests were performed by placing the substrates (5 mm diameter) in a 24-well tissue plate. Previously to the adsorption, samples were equilibrated in degassed PBS with 0.01 M NaI (PBSI) to prevent adsorption of free ^{125}I ions present in trace amounts in ^{125}I-FN. A drop of 10 μl of (^{125}I-FN) solution was added to each surface. Adsorption tests were carried out at 25 °C for 60 min. After this period the drop was absorbed from the surface with absorbent paper, and the surface was washed three times with PBS. In order to ensure that free ^{125}I and non-adsorbed protein are removed of the surfaces, the samples were kept in PBS for 24 h, washed in PBS (3×) and transferred to other radioimmunoassay tubes to measure the surface activity using an automatic gamma counter (model 1470 Wizard, from Wallac). All experiments were done in triplicate. The counts from each sample were averaged, and the surface concentration was calculated by the equation:

$$[\mathrm{FN}]\,(\mu\mathrm{g/m^2}) = \frac{[\mathrm{counts\,(cpm)}][[\mathrm{FN}]_{\mathrm{solution}}(\mu\mathrm{g/mL})]}{[A_{\mathrm{solution}}\,(\mathrm{cpm/mL})][\mathrm{SA\,(m^2)}]},$$

where the counts measure the radioactivity of the samples, $[FN]_{solution}$ is the FN concentration in solution, $A_{solution}$ is the specific activity of the FN solution, and SA is the surface area expressed as the area occupied by the drop during adsorption tests, measured by contact angle software.

Different FN concentrations 2, 10 and 20 μg/ml were studied on all the surfaces during 60 min. After FN adsorption, samples were immersed in fresh FN solutions (20 μg/ml) for 24 h. Then the surfaces were washed with PBS and the residual activity was measured in order to quantify the fraction of molecules that remains adsorbed on the different surfaces. Displacement tests were carried out by immersing the labelled surfaces over 24 h in an unlabelled FN pure solution. The substrates were washed three times with PBS, and the residual activity was counted.

2.4. Cell culture

MC3T3-E1 cells were obtained from the RIKEN CELL BANK (Japan). Prior to seeding on FN-coated substrates, cells were maintained in DMEM medium supplemented with 10% fetal bovine serum and 1% penicillin–streptomycin and passaged twice a week using standard techniques.

Sample disks (12 mm diameter) placed in a 24-well tissue culture plate were coated with FN 20 μg/ml (12 h at 37 °C). Then, 10^3 cells were placed onto each substrate and were maintained at 37 °C in a humidified atmosphere under 5% CO_2 for 3 h. Each experiment was performed in triplicate.

2.5. Cell adhesion

After 3 h of culture MC3T3-E1 cells were washed in Dulbecco's phosphate buffered saline (DPBS, Invitrogen) and fixed in 10% formalin solution (Sigma) at 4 °C for 1 h. Samples were then rinsed with DPBS and a permeabilization buffer (103 g/l sucrose, 2.92 g/l NaCl, 0.6 g/l $MgCl_2$, 4.76 g/l HEPES buffer, 5 ml/l Triton X-100, pH 7.2) was added at room temperature for 5 min. In order to reduce the background signal, samples were incubated in 1% BSA/DPBS at 37 °C for 5 min. Afterwards, samples were incubated in monoclonal mouse antibody against vinculin (1:400 in 1% BSA/DPBS; Sigma) at room temperature for 1 h. The samples were rinsed in 0.5% Tween 20/DPBS three times for 5 min each. Alexa fluor 633-conjugated rabbit anti-mouse secondary antibody (1:200 in 1% BSA/DPBS; Invitrogen) was then added at room temperature for 1 h. Simultaneously, BODIPY FL phallacidin was added for the duration of this incubation (2–3 units/sample in 1% BSA/PBS; Invitrogen). Finally, samples were washed before mounted in Vectashield containing DAPI (Vector Laboratories, Peterborough, UK). A Leica DM6000B fluorescent microscope was used for cellular imaging.

2.6. Fibronectin reorganisation and formation

The ability of cells to reorganise adsorbed FN (i.e. early matrix) was monitored by coating all samples with 20 μg/ml at 37 °C, then rinsing with PBS twice, before seeding in serum containing medium. The ability of cells to secrete and deposit FN into the extracellular matrix fibrils (i.e. late matrix) was examined via immunofluorescence. For that, cells were cultured on the different substrates for 3 h, 1, 3 and 6 days in serum containing medium.

The evolution of FN in the ECM was followed by immunofluorescence. At the end of incubation time, cells were washed in Dulbecco's phosphate buffered saline (DPBS, Invitrogen) and fixed in 10% formalin solution (Sigma) at 4 °C for 1 h. Samples were rinsed with DPBS and the permeabilization buffer was added at room temperature for 5 min. Samples were incubated with a polyclonal rabbit anti-FN antibody (1:400, Sigma), dissolved in 1% BSA/DPBS for 1 h, washed, and incubated with a goat anti-rabbit Cy3-conjugated secondary antibody for 1 h before washed and mounted with Vectashield containing DAPI.

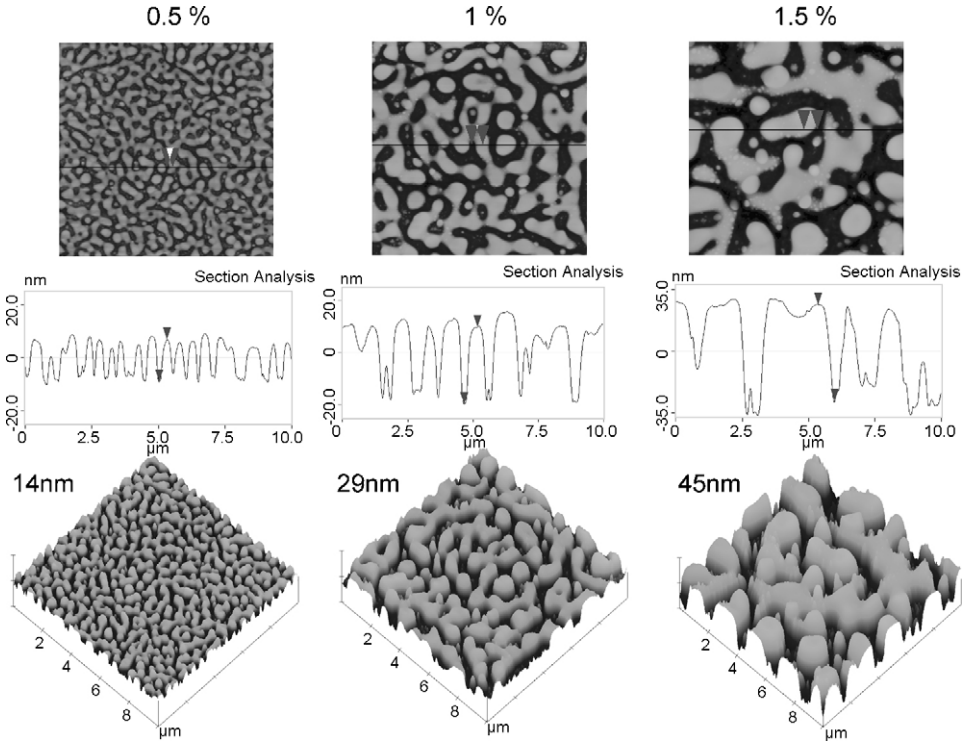

Fig. 1. AFM images for the PLLA/PS (50/50, w/w) demixed nanotopographies as obtained after spin casting from solutions of concentrations 0.5, 1 and 1.5 wt% in chloroform. The first row shows the height magnitude, the second one the transversal cut and the last one the 3D reconstruction of the surface.

2.7. Image analysis

All image processing and analysis was done using an in house software developed under MATLAB R2008a (The MathWorks, Inc., Natick, MA, USA).

For calculating the distribution of FN between valleys and pits, the valleys and the pits were firstly delineated. For this, the height AFM image was grayscaled and equalized, providing an output grayscale image with its intensity values evenly distributed throughout the intensity range, and then a median filtering was applied to the resulting image to reduce noise background. This new image was then binarized through Otsu's method [24], which chooses the threshold that minimizes the intraclass variance of the thresholded black and white pixels, providing a binary image with the valleys and the pits perfectly segmented. The contour of the pits was then easily extracted and applied, in a second step, to the amplitude and phase AFM images.

FN was detected from the amplitude and phase AFM images. It was afterwards associated to the valleys or to the pits based on the contour between both previously detected using the height AFM images, and the results were averaged. For this procedure, several steps were followed: (i) both images were firstly grayscaled, equalized and a median filtering was applied to the resulting images for a background noise reduction. The histogram of both images was then automatically stretched for a fair detection of the protein. The images were then size-filtered to avoid the detection of any too small region not corresponding to proteins. Once the protein was correctly detected, it was associated to a valley or to a pit based on the contour previously detected from the height AFM image. The resulting protein distribution was averaged between the amplitude and the phase images.

The size distribution of the focal plaques was determined through a several-step image analysis including a contour delineation of the cell. For a perfect segmentation of the cell: (i) Images showing the actin cytoskeleton were grayscaled and equalized. (ii) The cell was then detected (segmented): since the cytoskeleton differed greatly in contrast from the background image, a gradient-magnitude method (Sobel) [25–27] was applied to the image and once the gradient image was calculated, a binary mask was created containing the segmented cytoskeleton. (iii) Compared to the original image, the binary gradient mask showed gaps in the lines surrounding the cell (the outline of the object of interest was not completely delineated). These linear gaps disappeared when the Sobel image was dilated using linear structuring elements (a vertical structuring element followed by a horizontal one), obtaining a clear and perfect contour detection of the cell. Once the cell was perfectly segmented, the obtained binary mask was then applied to the image obtained in the red channel for vinculin. This permitted to focus the attention on the cell and the focal adhesions, as other any object in the image was virtually erased. This new image was then binarized through Otsu's method [24] and size-filtered to avoid any extra small particles in the image that did not represent focal plaques which sizes wanted to be determined. Once the sizes of the focal contacts were determined, a size distribution was easily obtained.

3. Results

3.1. Protein adsorption on nanoscale topographies

Fig. 1 shows AFM height images of PLLA/PS (50/50, w/w) nanotopographies as obtained by demixing during high-speed spin-casting on glass coverslips at various solutions concentrations in chloroform: 0.5% (14 nm deep pits), 1% (29 nm deep pits) and 1.5% (45 nm deep pits). The fraction of the area covered of pits does not depend on the individual topographic scale (approximately 32%). Also, the samples showed increased values for the real 3D surface area: 5 μm × 5 μm AFM images showed 25.15, 25.20 and 25.30 μm^2 for 14, 29 and 45 nm deep pits respectively. These values are in agreement with those reported previously for this system [14].

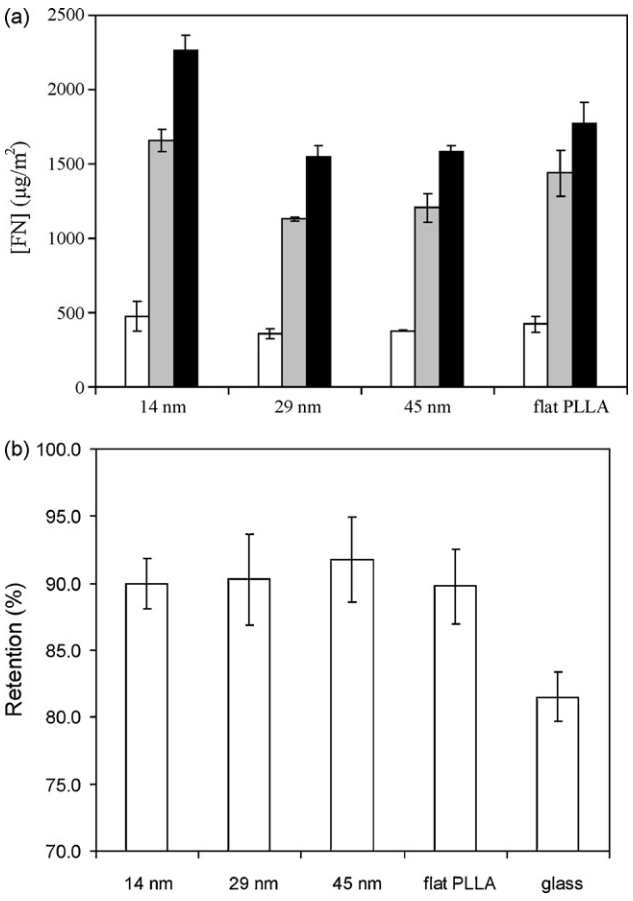

Fig. 2. Quantification of FN adsorption by radioactivity. (a) Surface density of FN after adsorption for 60 min on the different nanotopographies and flat PLLA from solutions of concentration 2 μg/ml (white), 10 μg/ml (gray), and 20 μg/ml (black). (b) Retention of FN molecules on the surface after 60 min of adsorption at 20 μg/ml and elution by other FN molecules, after 60 min of adsorption. The elution time was 24 h.

Fig. 2 shows the amount of FN adsorbed on the different substrates (the nanopits and flat PLLA) from solutions of different concentrations, i.e. 2, 10 and 20 μg/ml as obtained by radiolabelling of FN with ^{125}I (^{125}I-FN). For a fixed nanotopography, the amount of adsorbed FN increases as the concentration of the protein solution does. For a fixed concentration of the FN solution, the amount of adsorbed protein is higher on the 14 nm deep pits surface compared to the 29 and 45 nm deep pits nanotopographies on which the amount of adsorbed FN is similar. In concrete, when adsorbing from the 20 μg/ml FN solution – which is the concentration of the solution used in cell culture later on – 2250 μg/m^2 of the protein were adsorbed on the 14 nm deep pit surface which lowers to approximately 1500 μg/m^2 for the other two surfaces (29 and 45 nm deep pits). That is to say, the amount of adsorbed FN is approximately 50% higher on the 14 nm deep pit nanotopography.

The exchangeability of bound FN molecules was evaluated by the exchange of the preadsorbed ^{125}I-FN for unlabelled FN. Fig. 2b shows the percentage of ^{125}I-FN retained on the different surfaces after they were soaked in FN after 60 min of adsorption. The elution time was 24 h. It can be seen that all three nanotopographies and flat PLLA shows similar behavior and only approximately 10% of the initially adsorbed FN is eluted. The same experiment was done

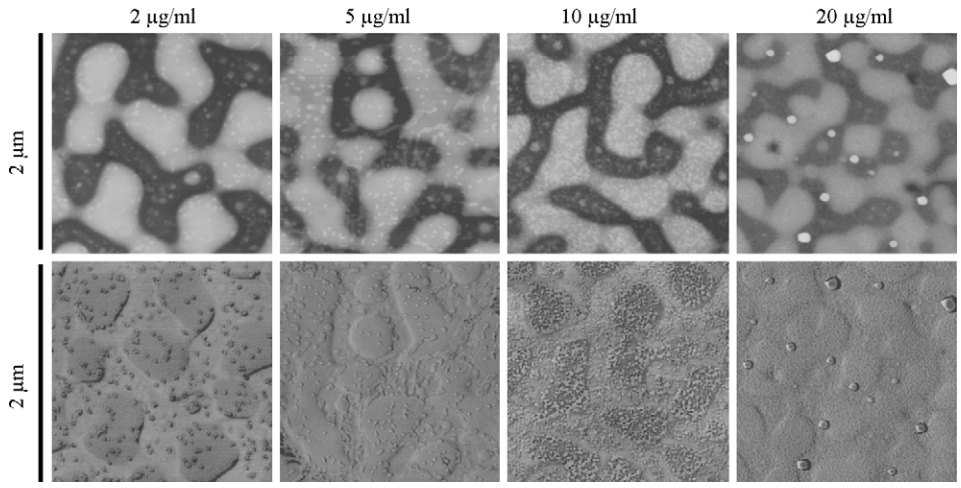

Fig. 3. Height (first row) and phase (second row) AFM magnitudes for the 14 nm deep pit nanotopography after FN adsorption from solutions of concentrations 2, 5, 10 and 20 μg/ml. The height magnitude allows one to identify the peaks and valleys in the surface while the phase magnitude provides direct observation of FN distribution throughout the sample.

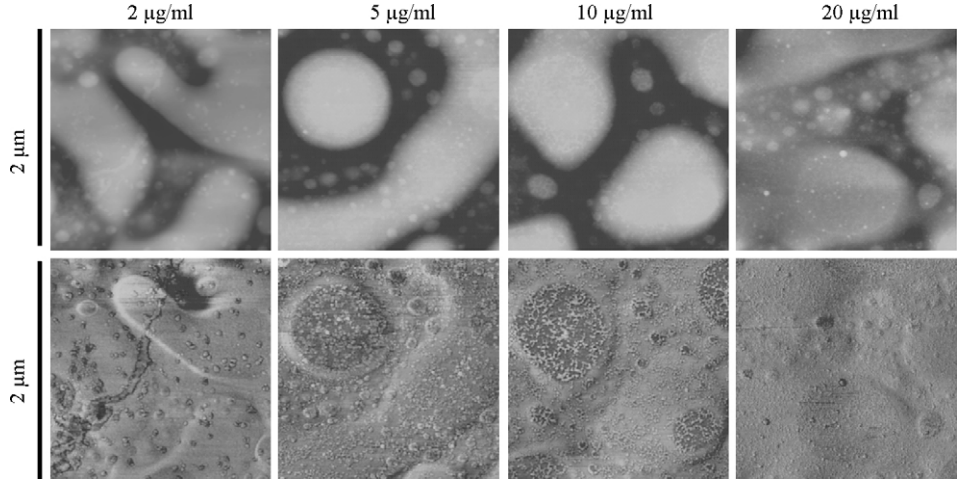

Fig. 4. Height (first row) and phase (second row) AFM magnitudes for the 29 nm deep pit nanotopography after FN adsorption from solutions of concentrations 2, 5, 10 and 20 μg/ml. The height magnitude allows one to identify the peaks and valleys in the surface while the phase magnitude provides direct observation of FN distribution throughout the sample.

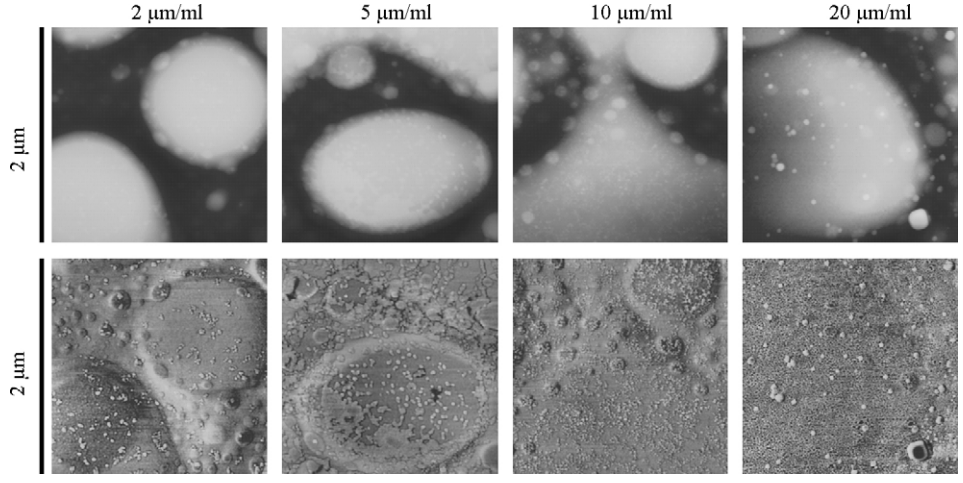

Fig. 5. Height (first row) and phase (second row) AFM magnitudes for the 45 nm deep pit nanotopography after FN adsorption from solutions of concentrations 2, 5, 10, and 20 μg/ml. The height magnitude allows one to identify the peaks and valleys in the surface while the phase magnitude provides direct observation of FN distribution throughout the sample.

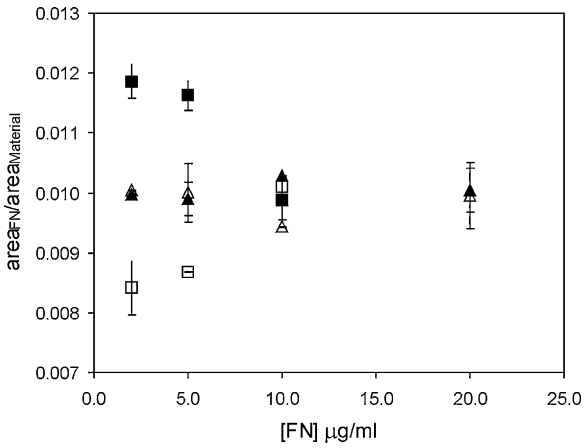

Fig. 6. Fraction of the area covered by FN as obtained from image analysis of the AFM images. It is shown the fraction occupied by the protein relative to the area of the peaks (empty symbols) and valleys (filled symbols). Squares: 14 nm deep pits nanotopographies; triangles: 29 and 45 nm deep pits nanotopographies.

on glass coverslips, and the fraction eluted from the surface was significantly higher, approximately 20%.

Figs. 3–5 show the AFM height and phase magnitudes for the different nanotopographies after FN adsorption from solutions of concentration 2, 5, 10 and 20 μg/ml respectively. FN molecules are better identified on the phase image, while the height magnitude can be used for identifying, simultaneously, the spatial distribution of FN throughout peaks and valleys in the sample. Only isolated molecules are observed after adsorption from the solution of concentration 2 μg/ml, which associate into small aggregates which results in a continuous protein layer on the sample after adsorption from solutions of higher concentrations (10 and 20 μg/ml respectively). Image analysis of the AFM figures allows one to quantify the distribution of molecules between pits and valleys of the nanostructure, after adsorption from solutions of different concentrations (Fig. 6). It is observed that, for the 14 nm deep pits, FN is preferentially adsorbed on the valleys of the nanostructure when the concentration of the solution is lower than 10 μg/ml. However, FN is evenly distributed between valleys and peaks of the samples when adsorbed from solutions of 10 and 20 μg/ml. FN distributes randomly between pits and valleys independently of the concentration of the solution when adsorbed on the 29 and 45 nm deep pits nanotopographies (Fig. 6).

3.2. Cell adhesion and FN matrix formation

Fig. 7 shows the overall morphology of cells adhering for 3 h on FN-coated nanotopographies and flat PLLA, visualised via staining for actin (left column). Cells presented prominent actin fibers inserting into well-developed focal adhesion complexes, as depicted in the central column for vinculin. It is clearly observed that the size of focal complexes increases from the 14 nm deep pits nanotopography to the 45 nm pits one, which can be quantified by image analysis. Fig. 8 shows the size distribution of focal adhesion complexes for the three nanotopographies. Small focal complexes

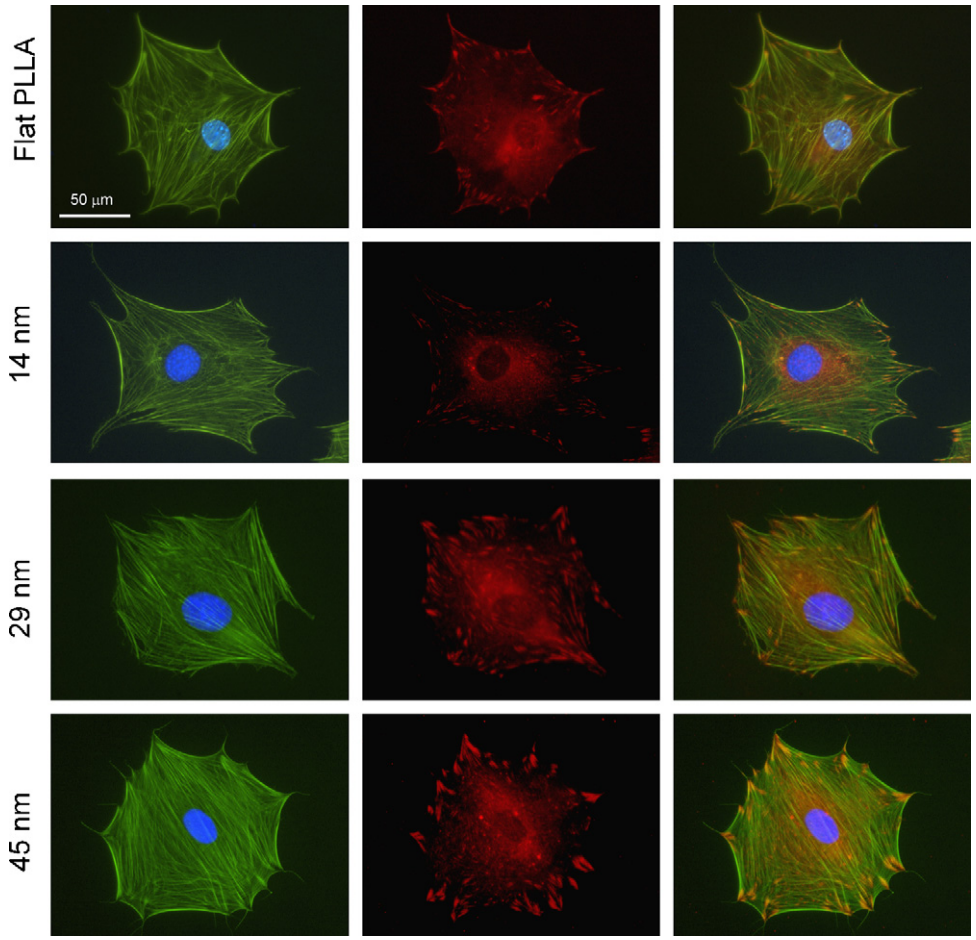

Fig. 7. MC3T3 osteoblast-like cells after 3 h on FN-coated nanotopographies. First column shows F-actin cytoskeleton and second one focal adhesion plaques (vinculin). The third column is the superposition of the other two. Nuclei were counterstained with DAPI.

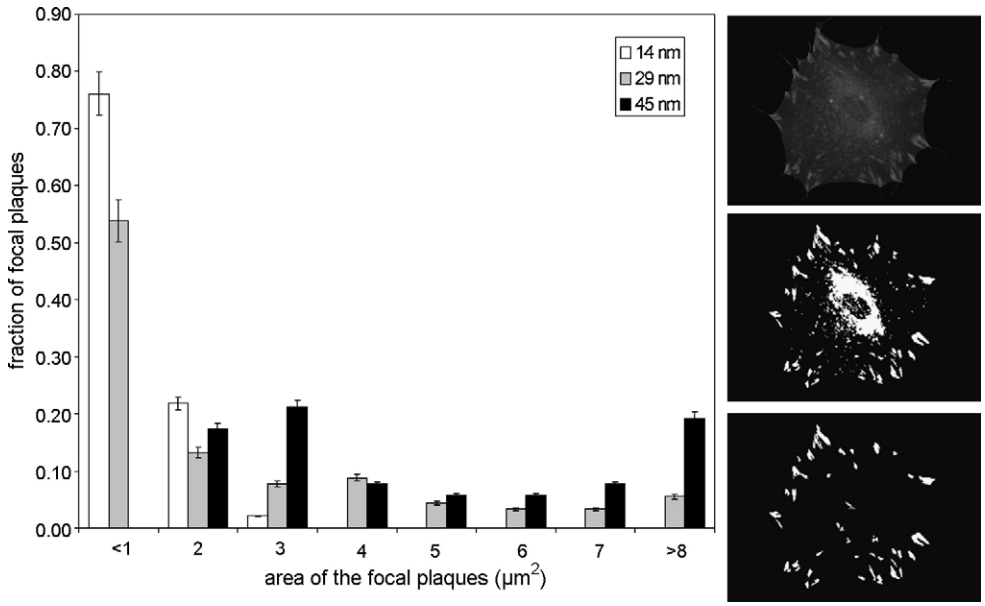

Fig. 8. Size distribution of focal adhesion plaques on each nanotopography as quantified by image analysis. The picture shows the sequential process described in the text to delimitate focal adhesion plaques from the original image.

are found for the 14 nm deep pits topographies, such that the whole distribution is below 3 μm^2 and 75% below 1 μm^2. The size distribution expands up to 8 μm^2 on the 29 nm deep pits, while still 70% of the values below 2 μm^2; the distribution is completely altered for the focal plaques formed on the 45 nm deep pits topography: there is no focal plaque smaller than 1 μm^2, 40% of them are in the range of 2–3 μm^2 and approximately 25% are larger than 1 μm^2 (Fig. 8).

Fig. 9 shows the cellular reorganisation of adsorbed FN after 3 h of culture for the different nanotopographies, flat PLLA and the control glass. It is observed that cells are able to reorganise FN on the control glass as it is shown by the dark area nearby the cell, specially when comparing the actin cytoskeleton (right column) and the staining for FN (left column). Reorganisation occurs much less actively for flat PLLA and the different nanotopographies. It is shown that some movements of the adsorbed FN layer takes place in any case but the dark areas in the pericellular zone are smaller and mostly coincident with focal adhesion plaques. Reorganisation is more important for the 29 and 45 nm deep pits nanotopographies and it is almost absent for the 14 nm deep pit structure (Fig. 9).

Fig. 10 shows late FN matrix formation for the different nanotopographies and flat PLLA after different culture times. It is observed that, as expected, matrix production increases as time goes by on every substrate. However, cells are able to synthesize and deposit FN matrix fibrils – more abundantly and better organized into fibrillar networks – for the 29 and 45 nm deep pits nanotopographies rather than the 14 nm deep pits one.

4. Discussion

Despite the belief that the cell–protein–material interaction is of fundamental importance for understanding the role of materials in biomedicine, clear links between the material surface properties, the adsorbed protein layer and their influence on the cell remain far from being understood. Even if some efforts have been devoted to the influence of some material properties (e.g. hydrophilicity), clear correlations between nanotopography, protein adsorption and cell behavior have not been established yet [28–33].

Phase separation during high-speed spin-casting process of PLLA/PS (50/50, w/w) solutions of different concentrations (0.5, 1 and 1.5 wt%) leads to well-defined surface nanotopographies (14, 29 and 45 nm deep pits topographies). Besides, since PLLA tends to segregate to the air–film interface, the system consists of different nanotopographies with the same surface chemistry [14,34]. That is to say, the system is appropriate for investigating the effect of surface nanotopography on the cell–protein–material interaction independently of the surface chemistry that is kept constant. This is an important matter since protein adsorption is mostly affected by the material surface and, consequently, cells are only sensitive to the topmost surface chemistry of the films. The layer of interest for protein adsorption and cell adhesion consists of PLLA nanopits of different sizes.

The effect of this concrete family of substrates on human fetal osteoblastic (hFOB) cells was previously investigated in the literature [14]. There, it was found that cell adhesion was enhanced on the 14 nm deep pits nanotopography, in agreement with other studies [35–37]. Moreover, focal adhesion development in hFOB was found to be enhanced on 14 and 29 nm pit surfaces; however, only paxillin expression was altered while vinculin did not display significantly altered expression with respect to nanopit textures [14]. However, our results show that vinculin distribution throughout the cell periphery is modified as a consequence of the underlying nanotopography (Fig. 7). Focal plaques are larger as the *z*-axis scale dimension of the structure increases, as it is quantified by the frequency distribution included in Fig. 8. This behavior must be a consequence of the availability of the adsorbed FN layer on the material surface which is influenced by the underlying nanotopography. It is important to remark here that our study was done in serum free conditions, which (i) is an important difference with respect to previous investigations on this family of nanotopographies [14] and (ii) allows one to characterise the cell–material interface in terms of the amount of FN adsorbed and its conformation, evaluating the specific cell–FN interaction. Not only the vertical size of the topography changes for the different substrates, but also the characteristic horizontal area of the pits which is approximately 0.08, 0.2 and 0.5 μm^2 for the 14, 29 and 45 nm deep pits nanotopographies respectively as it can be inferred from Figs. 1 and 3–5. The organisation of focal adhesion plaques must be dictated by the horizontal area of the pits on the material surface – correlated to the height of the nanopits – which tailor the size of focal adhesion sites (Fig. 8). It has been reported that cells

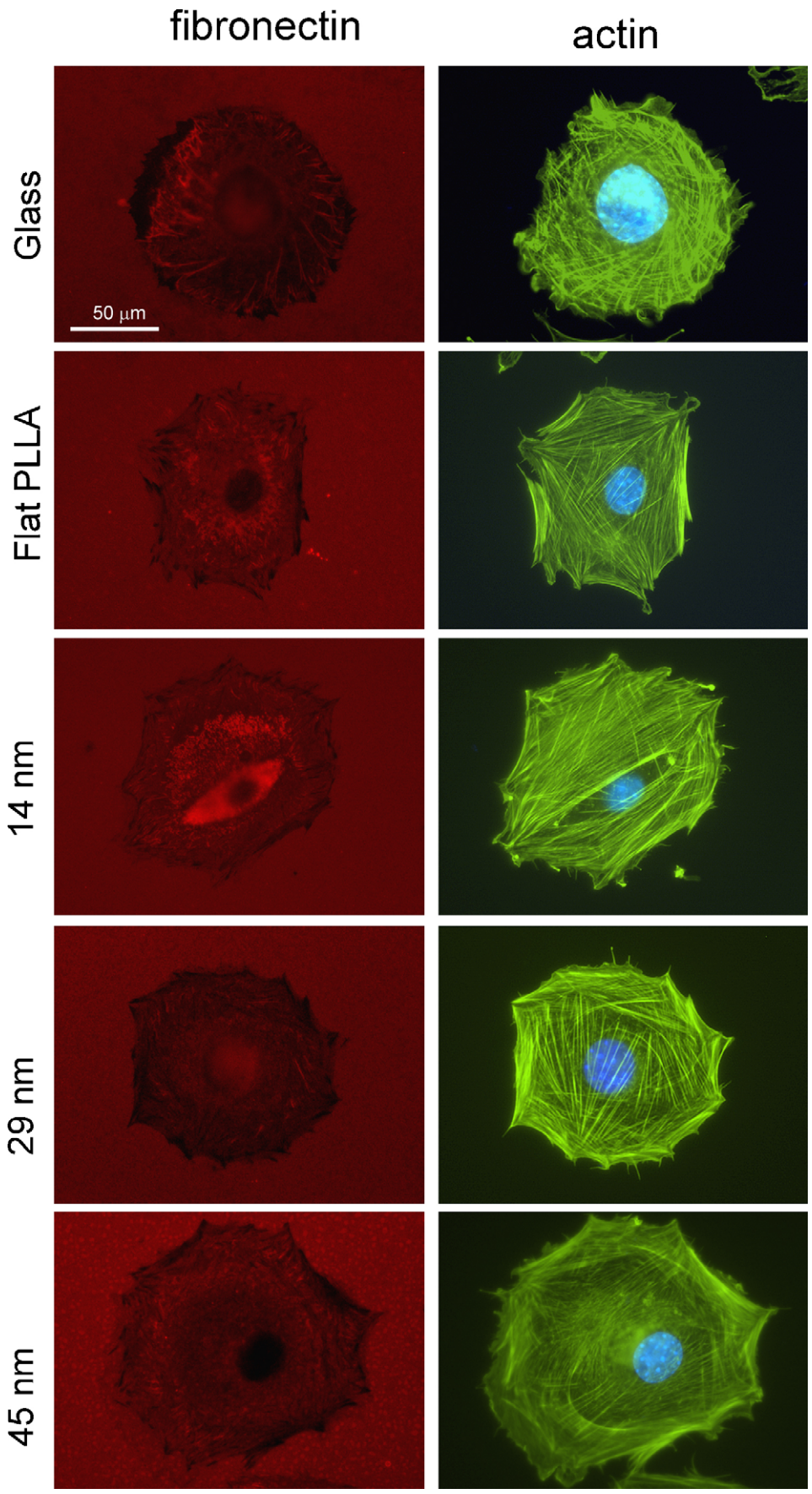

Fig. 9. Cellular reorganisation of adsorbed FN on the different nanotopographies, flat PLLA and glass. The F-actin cytoskeleton is also included for each cell. Nuclei were counterstained with DAPI.

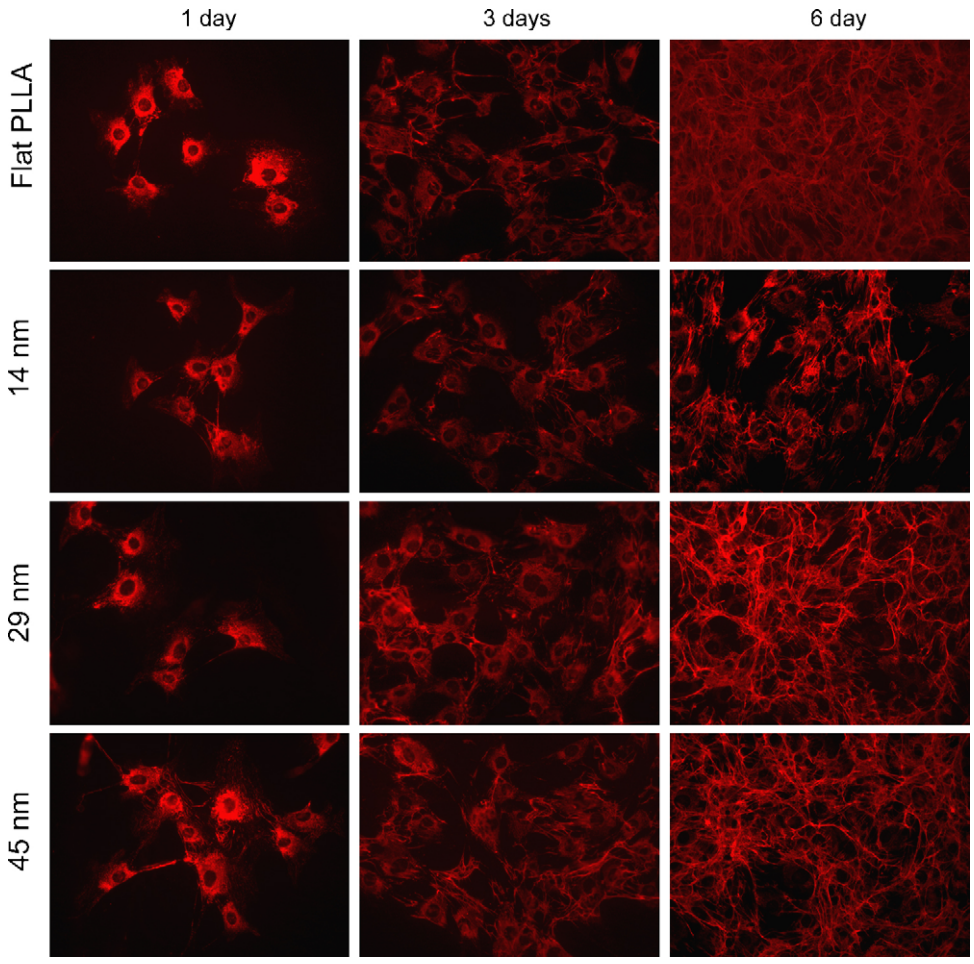

Fig. 10. Dynamics of fibronectin matrix formation on the different nanotopographies and the flat PLLA.

were able to form larger focal contacts on nanostructure materials [17]; but to our knowledge such a clear trend and its frequency distribution had not been reported so far. Vinculin level at adhesion sites has been correlated in a linear manner with tractional forces exerted by cells, so that tension needs to be developed between the ECM and the adhesion site for vinculin recruitment [38,39]. The formation of mature focal adhesions occurs through integrin clustering via increased force generated by the cytoskeleton [40]; the other way around, less mature cytoskeleton suggests that less tension is applied to integrins resulting in less clustering and smaller contacts [41]. We have not found any difference in the state of development of actin cytoskeleton on the different nanotopographies (Fig. 7) regardless the size of the focal contact plaques which suggests that the size of the adhesion contacts, being directly modulated by the available area on the nanopits, are large enough so as to allow cell adhesion and mechanotransduction via actin cables.

The amount of adsorbed FN depends on the topographical nanostructure of the substrate. FN adsorption is higher on the 14 nm deep pit surface than on the 29 and 45 nm pits surfaces. This phenomenon is remarkable since suggesting a direct influence of surface topography on protein adsorption (since the same surface chemistry is obtained for every substrate [14]). The origin of this fact cannot be explained by small differences in the real three-dimensional areas among nanotopographies (less than 3%). Besides, FN is equally distributed between pits and valleys after adsorption from a solution of concentration 20 μg/ml (Fig. 6) – the one used for coating samples before cell culture. This is not the case when FN is adsorbed on titanium microtopographies – from a solution concentration of 20 μg/ml – as it is preferentially adsorbed on topographic peaks [42]. It is suggested that the difference in the total amount of adsorbed FN does not influence the size of the focal plaques, since they are different in size on the 29 and 45 nm pits surfaces (Figs. 7 and 8) but similar FN density is found on them (Fig. 2). That is to say, vinculin distribution on the different nanotopographies must be a consequence of the local organisation (at the nanoscale) of the underlying material surface – which is covered by a uniform layer of the protein – considering both the vertical and horizontal dimensions of the pits, and not due to either (i) the difference in the amount of adsorbed protein (Fig. 2), or (ii) the influence of nanotopography on the conformation and distribution of the adsorbed FN molecules (Figs. 3–5).

Moreover, the size of the focal adhesion plaques is related to the ability of cells to rearrange the adsorbed protein layer. Fig. 9 shows that cellular reorganisation of adsorbed FN (black areas around the pericellular edge) takes place preferentially on the 29 and 45 nm deep pits nanotopographies, and it is almost absent on the 14 nm deep pits surface. FN reorganisation is more important on the underlying glass, a hydrophilic substrate that bounds proteins loosely and leads to strong cell rearrangement of the adsorbed protein layer [29]. Previous investigations have shown that for cells to remove and reorganize the adsorbed FN layer in matrix fibrils, material need to adsorb proteins loosely [43–46]. The strength of interaction between the adsorbed protein layer and the material surface is related to the exchangeability of FN molecules by other FN molecules or other protein after adsorption [47]. In our case, the strength of interaction between the adsorbed FN molecules and the underlying substrate must be similar for each nanotopography, since the elution of bound FN molecules showed no differences

among the different substrates – Fig. 2b (FN elution is higher on glass which means lower strength of adhesion and higher cellular reorganisation).

There are topological constraints for cells to reorganize the adsorbed FN layer due to vertical and the horizontal dimensions of the underlying nanopits. It has been reported that the (micro)topography of titanium influences the presence of fibrillar adhesions [48] (i.e. extracellular matrix fibrils reorganised by cells [49]). Matrix reorganisation takes place via integrin–FN interaction, involving the transmission of forces from the actin cytoskeleton to the ECM via focal adhesion plaques [41]. We have found that, even if PLLA is a material on which FN reorganisation is highly difficult (Fig. 9), the presence of nanopits provides some degrees of freedom for cell-mediated FN rearrangements, the more the larger the nanopit size (Fig. 9).

Late FN matrix formation, after different time periods (Fig. 10), is enhanced on the 29 and 45 nm deep pits nanotopographies, i.e. on the substrates on which FN reorganisation takes place more intensively. Cells are able to secrete their own extracellular matrix on flat PLLA, but matrix deposition is strongly affected by substrate's nanostructure. Scarce FN formation is obtained when cells are seeded on the 14 nm deep pits nanotopography. This must be related to the fact that matrix reorganisation is almost absent on this surface. On the contrary, when the initial FN layer is reorganised by the adhered cell, FN formation takes place more abundantly. This fact suggests that late matrix formation is in need not only of cell adhesion on the substrate, but some cell movements, in the range of the size of the focal adhesion plaques, must take place so matrix deposition takes place normally. Late matrix formation has been related to the ability of cells to rearrange the initially adsorbed protein layer, especially when comparing cell adhesion on hydrophilic and hydrophobic substrates [44,46,50].

5. Conclusions

Our results suggest the importance of the adsorbed FN layer in cellular response to different nanotopographies. We have found that FN adsorption depends on the size of the nanostructure, i.e. the amount of adsorbed FN is higher on the 14 nm deep substrate than the other two ones (29 and 45 nm deep pits). However, protein conformation and distribution between valleys and peaks is similar when FN adsorption takes place from solutions of concentration of 10 μg/ml or higher. Moreover, the distribution of focal adhesions (vinculin) is strongly affected by the size of the nanopits. When focal adhesion plaques are too small, even if cells are able to adhere on the substrate and they develop the actin cytoskeleton, there is no trace of reorganisation for the adsorbed FN layer which, in the long term, leads to diminishing functionality in the formation of the new matrix.

Acknowledgements

AFM was performed under the technical guidance of the Microscopy Service at the Universidad Politécnica de Valencia, whose advice is greatly appreciated. The support of the Spanish Ministry of Science through project MAT2009-14440-C02-01 (including the FEDER financial support) is kindly acknowledged.

References

[1] J. Spie, Ann. N. Y. Acad. Sci. 961 (2002) 1.
[2] L. Griffin, G. Naughton, Science 259 (2002) 1009.
[3] F. Grinnell, J. Cell Biol. 103 (1986) 2697.
[4] R.O. Hynes, Cell 110 (2002) 673.
[5] J.Y. Wong, J.B. Leach, X.Q. Brown, Surf. Sci. 570 (2004) 119.
[6] U.S. Schwarz, I.B. Bischofs, Med. Eng. Phys. 27 (2005) 763.
[7] P.T. Ohara, R.C. Buck, Exp. Cell Res. 121 (1979) 235.
[8] J.Y. Lim, H.J. Donahue, Tissue Eng. 13 (2007) 1879.
[9] S. Affrossman, R. Jerome, S.A. O'Neill, T. Schmitt, M. Stamm, Colloid Polym. Sci. 278 (2000) 888.
[10] F.A. Denis, P. Hanarp, D.S. Sutherland, Y.F. Dufrene, Nanoletters 2 (2002) 1419.
[11] C. Vieu, F. Carcenac, A. Pepin, Y. Chen, M. Mejias, A. Lebib, L. Manin-Ferlazzo, L. Couraud, H. Launois, Appl. Surf. Sci. 164 (2000) 111.
[12] R. Kriparamanan, P. Aswath, A. Zhou, L. Tang, K.T. Nguyen, J. Nanosci. Nanotechnol. 6 (2006) 1905.
[13] M.J. Dalby, D. Giannaras, M.O. Riehle, N. Gadegaard, S. Affrossman, A.S.G. Curtis, Biomaterials 25 (2004) 77.
[14] J.Y. Lim, D. Dreiss, Z. Zhou, J.C. Hansen, C.A. Siedlecki, R.W. Hengstebeck, J. Cheng, N. Winogard, H.J. Donahue, Biomaterials 28 (2007) 1787.
[15] M.J. Dalby, A. Hart, S.J. Yarwood, Biomaterials 29 (2008) 282.
[16] O. Zinger, G. Zhao, Z. Schwartz, J. Simpson, M. Wieland, D. Landlolt, B. Boyan, Biomaterials 26 (2005) 1837.
[17] M.J. Dalby, N. Gadegaard, R. Tare, A. Andar, M.O. Riehle, P. Herzyk, C.D.W. Wilkinson, R.O.C. Oreffo, Nat. Mater. 9 (2007) 997.
[18] M.J. Dalby, D. McCloy, M. Robertson, C.D.W. Wilkinson, R.O.C. Oreffo, Biomaterials 27 (2006) 1306.
[19] A. Pirouz-Dolatshahi, K. Rechendorff, M.B. Hovgaard, M. Foss, J. Chevallier, F. Besenbacher, Colloid Surf. B 66 (2008) 53.
[20] H.L. Khor, H. Kukula, K. Tamada, W. Knoll, M. Moeller, D.W. Hutmacher, Biomacromolecules 8 (2007) 1530.
[21] K. Cai, J. Bossert, K. Jandt, Colloid Surf. B 49 (2006) 136.
[22] Iodine-125, Amersham International, Little Chalfont, Buckinghamshire, U.K., 1993, p. 64.
[23] S.R. Sousa, M. Brás, P. Moradas-Ferreira, M.A. Barbosa, Langmuir 23 (2007) 7046.
[24] N.A. Otsu, IEEE Trans. Syst. Man Cybern. 9 (1979) 62.
[25] R.C. Gonzalez, R.E. Woods, S.L. Eddins, Digital Image Processing Using MATLAB, Prentice-Hall, Upper Saddle River, NJ, 2003.
[26] R.C. Gonzalez, R.E. Woods, Digital Image Processing, Prentice-Hall, Upper Saddle River, NJ, 2007.
[27] MATLAB Image Processing Toolbox User's Guide, The MathWorks, Inc., Natick, MA, 2006.
[28] L.T. Allen, M. Tosetto, I.S. Miller, D.P. O'Connor, S.C. Penney, I. Lynch, A.K. Keenan, S.R. Pennington, K.A. Dawson, W.M. Gallagher, Biomaterials 27 (2006) 3096.
[29] D. Gugutkov, G. Altankov, J.C. Rodríguez Hernández, M. Monleón Pradas, M. Salmerón Sánchez, J. Biomed. Mater. Res. A 92 (2010) 322.
[30] P. Rico, J.C. Rodríguez Hernández, D. Moratal, M. Monleón Pradas, M. Salmerón Sánchez, Macromol. Biosci. 9 (2009) 766.
[31] B.G. Keselowsky, D.M. Collard, A.J. García, J. Biomed. Mater. Res. A 66 (2003) 247.
[32] M.H. Lee, P. Ducheyne, L. Lynch, D. Boettiger, R.J. Composto, Biomaterials 27 (2006) 1907.
[33] E. Costa Martínez, J.C. Rodríguez Hernández, M. Machado, J. Mano, J.L. Gómez Ribelles, M. Monleón Pradas, M. Salmerón Sánchez, Tissue Eng. 14 (2008) 1751.
[34] J.Y. Lim, J.C. Hansen, C.A. Siedlecki, R.A. Hengstebeck, J. Cheng, N. Winograd, Biomacromolecules 6 (2005) 3319.
[35] X. Liu, J.Y. Lim, H.J. Donahue, R. Dhurjati, A.M. Maestro, E.A. Vogler, Biomaterials 28 (2007) 4535.
[36] M.J. Dalby, S.J. Yarwood, M.O. Riehle, H.J. Johnstone, S. Affressman, A.S. Curtis, Exp. Cell Res. 276 (2002) 1.
[37] M.J. Dalby, S. Childs, M.O. Riehle, H.J.H. Johnston, S. Affrossman, Biomaterials 24 (2003) 927.
[38] M.J. Dalby, D. McCloy, M. Robertson, H. Agheli, D. Sutherland, S. Affrossman, R.O.C. Oreffo, Biomaterials 27 (2006) 2980.
[39] M.J. Dalby, Med. Eng. Phys. 27 (2005) 730.
[40] C.G. Galbraith, K.M. Yamada, M.P. Sheetz, J. Cell Biol. 159 (2002) 695.
[41] N.Q. Balaban, U.S. Schwarz, D. Riveline, P. Goichberg, G. Tzur, I. Sabanay, Nat. Cell Biol. 3 (2001) 466.
[42] M. Pegueroles, C. Aparicio, M. Bosio, E. Engel, F.J. Gil, J.A. Planell, G. Altankov, Acta Biomater. (in press).
[43] G. Altankov, T. Groth, J. Mater. Sci. Mater. Med. 5 (1994) 732.
[44] G. Altankov, T. Groth, J. Mater. Sci. Mater. Med. 7 (1996) 425.
[45] G. Altankov, F. Grinnell, T. Groth, J. Biomed. Mater. Res. 30 (1996) 385.
[46] R. Tzoneva, T. Groth, G. Altankov, D. Paul, J. Mater. Sci. Mater. Med. 13 (2002) 1235.
[47] I.C. Gonçalves, M.C.L. Martins, M.A. Barbosa, B.D. Ratner, Biomaterials 26 (2005) 3891.
[48] F. Luthen, R. Lange, P. Becker, J. Rychly, U. Beck, J.G.B. Nebe, Biomaterials 26 (2005) 2423.
[49] B. Geiger, A. Bershadsky, R. Pankov, K.M. Yamada, Nat. Rev. Mol. Cell Biol. 2 (2001) 793.
[50] G. Altankov, T. Groth, J. Biomater. Sci. Polym. Ed. 8 (1996) 299.